Typeset using LaTeX **twocolumn** style in AASTeX62

School of Astronomy and Space Science, Nanjing University, Nanjing 210046, China
Key Laboratory of Modern Astronomy and Astrophysics (Nanjing University), Ministry of Education, Nanjing 210046, China
Department of Astronomy, University of Illinois at Urbana-Champaign, Urbana, IL 61801, USA
National Center for Supercomputing Applications, University of Illinois at Urbana-Champaign, 605 East Springfield Avenue, Champaign, IL 61820, USA
Harvard-Smithsonian Center for Astrophysics, 60 Garden Street, Cambridge, MA 02138, USA

houmc@smail.nju.edu.cn, xinliuxl@illinois.edu

Alfred P. Sloan Research Fellow

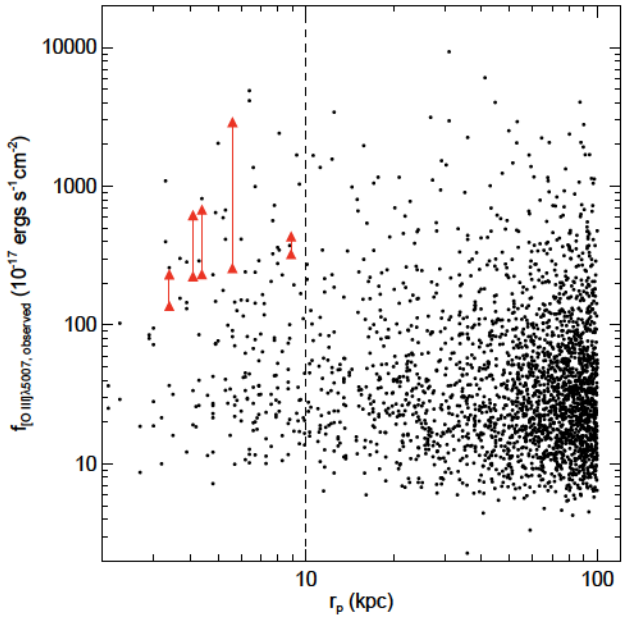

Figure 1. [O III] flux vs. projected separation r_p for our five target pairs and parent sample of 1286 AGN pairs (Liu et al. 2011) in red triangles and black dots, respectively. Our five targets are selected by requiring $r_p < 10$ kpc and both nuclei have sufficiently high [O III] fluxes. The vertical dashed line marks the position of $r_p = 10$ kpc.

lar [O III] fluxes, targets which are classified as Seyferts based on the BPT diagram are prioritized over those that are classified as AGN-H II composites to maximize the probability of X-ray detections. Therefore, our final target sample consists of five dual AGN candidates. The distribution of our sample is shown in Figure 1. Tables 1 and 2 list their basic photometric and spectroscopic properties. The stellar velocity dispersion was measured by fitting the host-galaxy stellar continuum using the penalized Pixel-Fitting (pPXF) method (Cappellari & Emsellem 2004) (see the Appendix for details). The total stellar mass was given by the MPA-JHU DR7 catalog from fitting the photometry (Kauffmann et al. 2003a; Salim et al. 2007). Figure 3 shows the narrow emission-line ratios measured from the SDSS spectra subtracted for stellar continua using the pPXF fits. It illustrates that the nuclei in our targets are optically classified as Type 2 Seyferts, LINERs, or AGN-H II composites.

3. OBSERVATIONS, DATA REDUCTION, AND DATA ANALYSIS

3.1. *Chandra ACIS X-ray Imaging Spectroscopy*

We observed the five dual-AGN candidates with the ACIS-S on board the *Chandra* X-ray Observatory between 2012 December and 2013 April (Program GO-14700264, PI: X. Liu). All targets were observed on-axis on the S3 chip, 5.2″ to 15.0″ away from the aimpoint. Each target was observed for 15 ks (Table 3). The exposure time was set to obtain ∼50 counts in the 2–10 keV range from the [O III] weaker nucleus in each merger, although the estimate was too optimistic. We estimated the X-ray counts from the [O III] luminosity for each nucleus (corrected for [O III] emission due to star formation in AGN-H II composites (Kauffmann & Heckman 2009)), assuming an empirical correlation between the 2–10 keV (unabsorbed) and [O III] luminosities. Measurements of $L_{2-10\,\mathrm{keV}}/L_{[O\,III]}$ for optically selected Type 2 AGNs span a wide range (Mulchaey et al. 1994; Heckman et al. 2005; Panessa et al. 2006), with values from a few to a few hundred. For the baseline assumption, we adopted the mean calibration of Panessa et al. (2006) given by,

$$\log\left[\frac{L_{2-10\,\mathrm{keV}}}{\mathrm{erg\,s^{-1}}}\right] = (1.22\pm0.06)\log\left[\frac{L_{[O\,III]}}{\mathrm{erg\,s^{-1}}}\right]+(-7.34\pm2.53), \quad (1)$$

where the [O III] luminosities have been corrected for the Galactic and intrinsic NLR extinction by using the Balmer decrement method via Hα/Hβ ratio. We accounted for systematic uncertainties using the Heckman et al. (2005) relation based on optically selected (single) Type 2 AGNs. An X-ray power-law spectrum was assumed with an absorbing column density $N_H = 10^{22}$ cm^{-2} (typical for our targets for which enough counts were detected for spectral analysis (see below) and for Type 2 Seyferts; Bassani et al. 1999) and a photon index $\Gamma = 1.7$ (typical for unabsorbed Seyferts; Green et al. 2009).

We reprocessed the data using CIAO v4.8 and the corresponding calibration files following standard procedure[1]. We examined the light curve of each observation and found no time interval of high background. We produced counts and exposure maps with the original pixel scale (0.″492 pixel^{-1}) in the 0.5–2 keV (S), 2–8 keV (H), and 0.5–8 keV (F) bands. The exposure maps were weighted by the above fiducial incident spectrum.

Following the source detection procedure detailed in Wang (2004) and Hou et al. (2017), we detect X-ray sources in the S, H and F bands in each image. With a local false detection probability $P \leq 10^{-6}$ (empirically yielding ∼0.1 false detection per field), we detected a total of 124 sources in the field-of-view covered by the S3 and S2 CCDs. For each detected source, we derived background-subtracted and exposure map-corrected count rates in each individual band from within the 90% enclosed-energy radius (EER), taking into account the position-dependent point-spread function and the local background.

[1] http://cxc.harvard.edu/ciao/

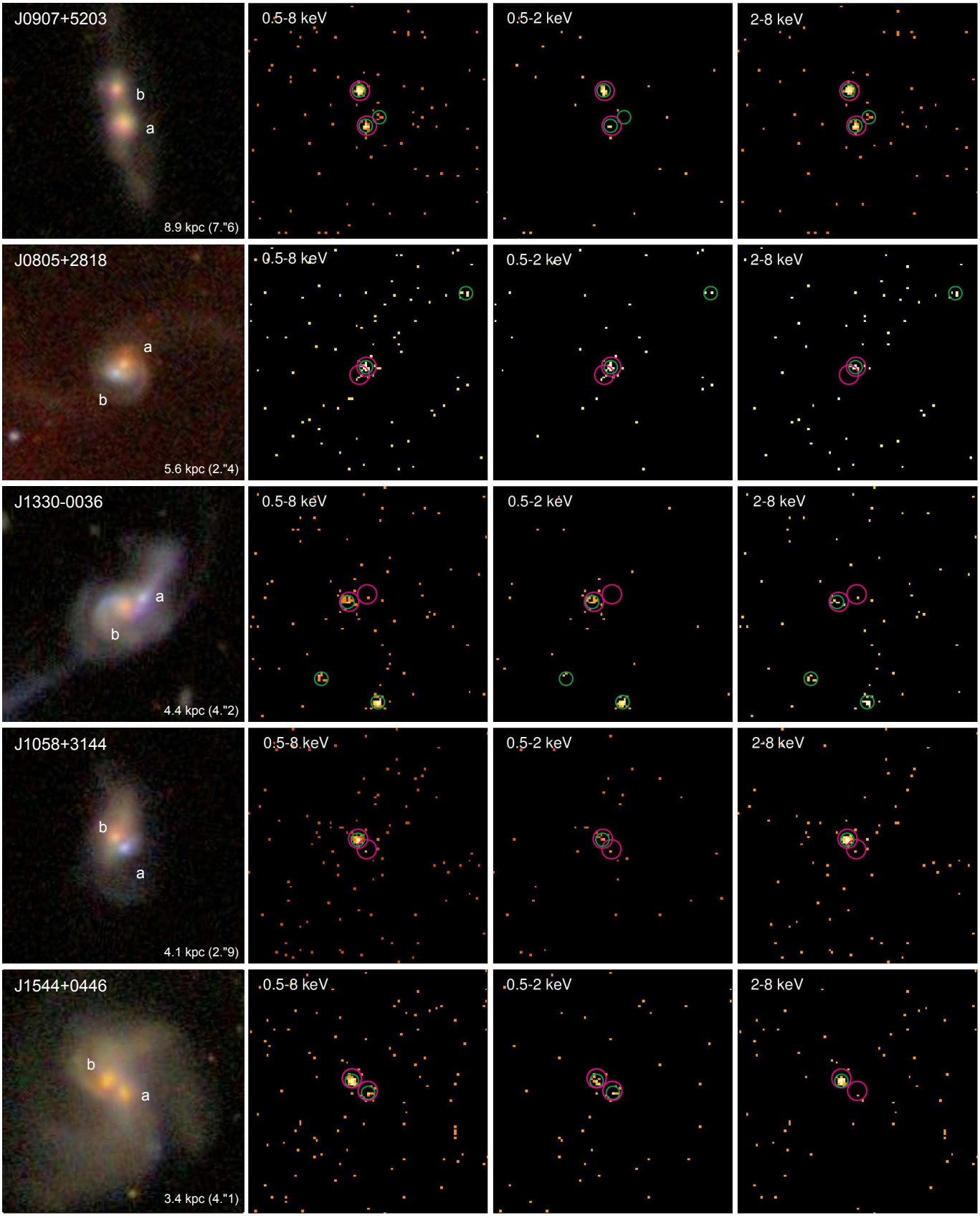
J0907+5203
b
a
8.9 kpc (7."6)
0.5-8 keV
0.5-2 keV
2-8 keV
J0805+2818
a
b
5.6 kpc (2."4)
0.5-8 keV
0.5-2 keV
2-8 keV
J1330-0036
a
b
4.4 kpc (4."2)
0.5-8 keV
0.5-2 keV
2-8 keV
J1058+3144
b
a
4.1 kpc (2."9)
0.5-8 keV
0.5-2 keV
2-8 keV
J1544+0446
b
a
3.4 kpc (4."1)
0.5-8 keV
0.5-2 keV
2-8 keV

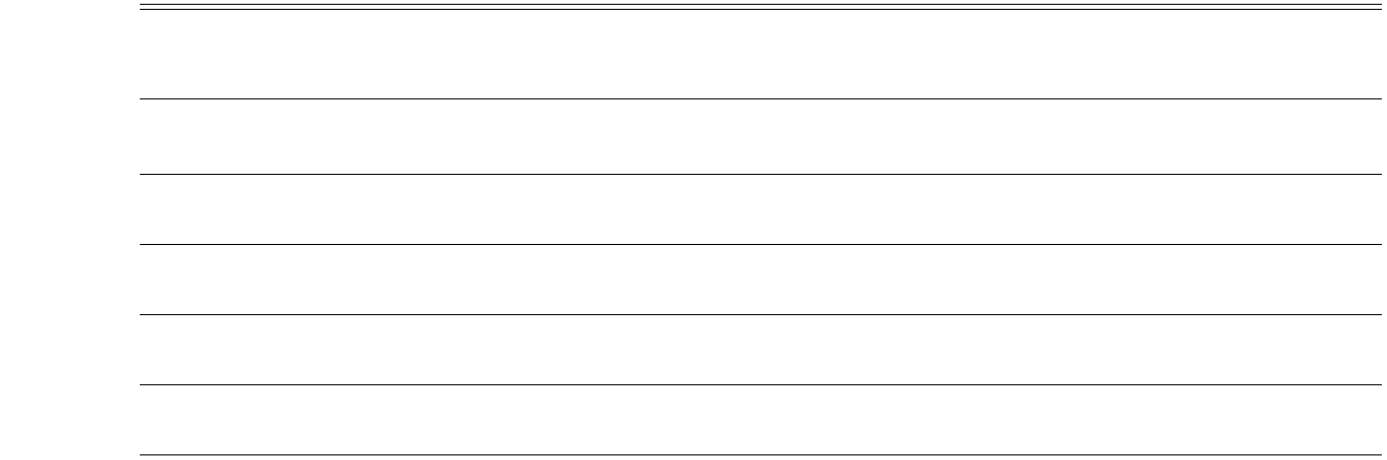

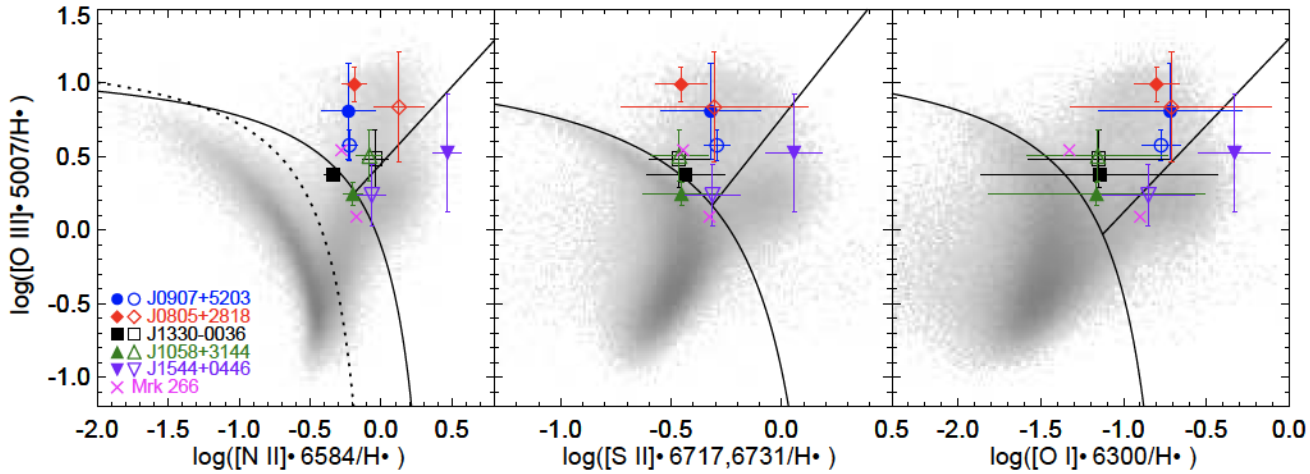

Figure 3. Optical diagnostic emission-line ratios (Baldwin et al. 1981; Veilleux & Osterbrock 1987) of the 10 nuclei in our five dual AGN candidates (colored solid symbols) and of the two nuclei in Mrk 266 (red crosses). Gray scales indicate number densities of SDSS DR4 emission-line galaxies (Kauffmann et al. 2003b). The dashed curve denotes the empirical separation between H II regions and AGNs (Kauffmann et al. 2003b), the solid curve displays the theoretical "starburst limit" (Kewley et al. 2001), and the solid line represents the empirical division between Seyferts and LINERs (Kewley et al. 2006). Pure star-forming ("SF") galaxies lie below the dashed curve, AGN-dominated objects (Seyferts above and LINERs below the solid line) lie above the solid curve, and AGN-H II composites lie in between.

Table 3. *Chandra* Observations of the Five [O III]-Selected Dual AGN Targets.

Name	ObsID	Exp.	Counts	CR	CR1	CR2	HR	Γ	N_H
(1)	(2)	(3)	(4)	(5)	(6)	(7)	(8)	(9)	(10)
J0907+5203a	14965	14.5	33.9	2.76 ± 0.44	0.33 ± 0.15	2.43 ± 0.42	$0.76^{+0.12}_{-0.10}$	-	-
J0907+5203b*	14965	14.5	108.9	7.63 ± 0.73	1.57 ± 0.32	6.06 ± 0.66	$0.56^{+0.08}_{-0.07}$	$1.43^{+0.84}_{-0.75}$	$2.6^{+1.5}_{-1.1}$
J0805+2818a	14964	14.0	28.9	2.04 ± 0.38	1.16 ± 0.28	0.89 ± 0.26	$-0.17^{+0.18}_{-0.19}$	-	-
J0805+2818b	14964	14.0	< 12.4	< 0.87	< 0.88	< 0.45	-	-	-
J1330−0036a	14967	14.9	< 8.4	< 0.57	< 0.43	< 0.59	-	-	-
J1330−0036b	14967	14.9	15.9	1.05 ± 0.27	0.57 ± 0.19	0.48 ± 0.18	$-0.13^{+0.27}_{-0.28}$	-	-
J1058+3144a	14966	14.5	< 12.1	< 0.81	< 0.72	< 0.57	-	-	-
J1058+3144b*	14966	14.5	79.8	5.99 ± 0.66	0.26 ± 0.13	5.73 ± 0.64	$0.91^{+0.05}_{-0.04}$	$1.13^{+1.64}_{-1.50}$	$6.4^{+6.3}_{-4.5}$
J1544+0446a	14968	14.9	5.8	0.38 ± 0.16	0.32 ± 0.14	< 0.58	$-0.62^{+0.09}_{-0.38}$	-	-
J1544+0446b*	14968	14.9	49.9	3.93 ± 0.52	0.45 ± 0.17	3.48 ± 0.49	$0.76^{+0.10}_{-0.08}$	$1.66^{+1.47}_{-1.35}$	$3.9^{+3.2}_{-2.7}$

NOTE—* represent the targets with sufficient net counts for spectral analysis (see Section 3.2). (2) *Chandra* observation ID; (3) *Chandra* effective exposure, in units of ks; (4) Observed net counts in 0.5-8 keV band; (5)-(7) Observed count rate in 0.5-8 (F), 0.5-2 (S) and 2-8 (H) keV bands, in units of 10^{-3} counts s^{-1}; (8) Hardness ratio, defined as $HR = (H - S)/(H + S)$; (9) Best-fitted photon index of a power-law model; (10) Best-fitted intrinsic column density of a power-law model, in units of 10^{22} cm^{-2}.

Figure 2 shows the ACIS images of the five targets in the F, S and H bands. Table 3 summarizes the X-ray measurements. Given the low count levels, we do not apply any smoothing to avoid artifacts. As we will show in Section 4.1, our targets are significantly weaker hard X-ray emitters than those predicted from both the Panessa et al. (2006) and Heckman et al. (2005) relations based on single optically selected AGNs, resulting in far fewer counts than expected. Seven of the ten nuclei in our targets were detected in the F-band. Six nuclei were detected in both S and H bands, whereas one nucleus (J1544+0446a) was detected in the S band only. Three nuclei (J0805+2818b, J1330−0036a and J1058+3144a) were undetected in the X-rays.

3.2. *Spectral Analysis and Hardness Ratio*

Three of the seven X-ray detected nuclei have sufficient net counts (≥50) for spectral analysis. For these nuclei, we extracted spectra from within the 90% EER of

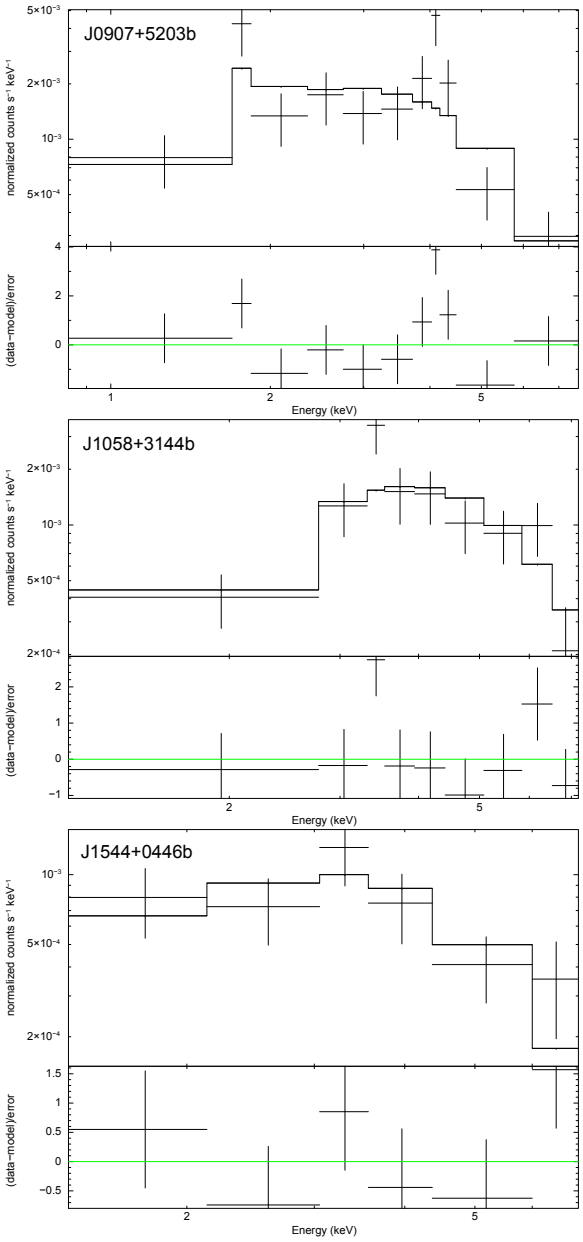
J0907+5203b
normalized counts s⁻¹ keV⁻¹
(data−model)/error
Energy (keV)
J1058+3144b
normalized counts s⁻¹ keV⁻¹
(data−model)/error
Energy (keV)
J1544+0446b
normalized counts s⁻¹ keV⁻¹
(data−model)/error
Energy (keV)

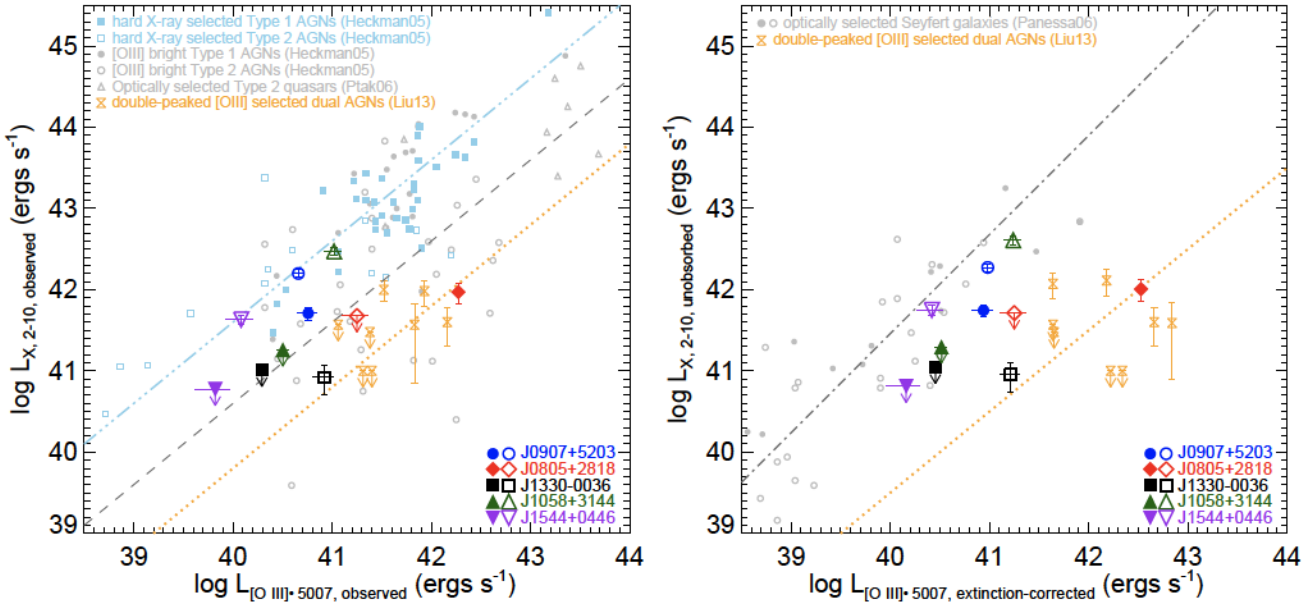

Figure 5. Hard X-ray luminosities vs. [O III] luminosities. Left panel: observed 2-10 keV luminosity vs. observed [O III] luminosity. For comparison, hard X-ray selected AGNs, [O III] bright AGNs (Heckman et al. 2005), optically selected Type 2 quasars (Ptak et al. 2006) and double-peaked [O III]-selected dual AGN sample of Liu et al. (2013) are shown in sky blue squares (Type 1s as filled and Type 2s as open), grey circles (Type 1s as filled and Type 2s as open), grey open upward triangles and yellow hourglasses, respectively. The mean relation for hard X-ray selected AGNs (both Type 1 and Type 2) and optically selected Type 1 AGNs (Heckman et al. 2005), optically selected Type 2 AGNs (Heckman et al. 2005) and double-peaked [O III]-selected dual AGNs (Liu et al. 2013) are shown in blue dashed-dotted-dotted, grey dashed and yellow dotted lines. Right panel: unabsorbed 2-10 keV luminosity vs. extinction-corrected [O III] luminosity. For comparison, nearby optically selected Seyfert galaxies (Panessa et al. 2006) are shown in grey circles. The grey dashed-dotted line is the mean relation for mixed Seyferts in nearby galaxies (Panessa et al. 2006) and the yellow dotted line is that for double-peaked [O III]selected dual AGNs (Liu et al. 2013).

Table 4. X-ray Luminosity of the Five [O III]-Selected Dual AGN Targets.

Name	$\log L_{X,0.5-8}$	$\log L_{X,0.5-2}$	$\log L_{X,2-10}$	$\log L_{X,2-10,\rm obs}$	$\log L_{[\rm O\,III],obs}$	$\log L_{[\rm O\,III],cor}$	SFR	$\log L^{\rm SF}_{0.5-2}$	$\log L^{\rm SF}_{2-10}$
(1)	(2)	(3)	(4)	(5)	(6)	(7)	(8)	(9)	(10)
J0907+5203a	$41.67^{+0.08}_{-0.06}$	$40.68^{+0.26}_{-0.16}$	$41.75^{+0.08}_{-0.07}$	$41.71^{+0.08}_{-0.07}$	$40.76^{+0.09}_{-0.11}$	$40.94^{+0.09}_{-0.11}$	$0.59^{+1.61}_{-0.52}$	$39.42^{+0.57}_{-0.94}$	$39.47^{+0.57}_{-0.94}$
J0907+5203b*	$42.35^{+0.04}_{-0.04}$	$41.89^{+0.10}_{-0.08}$	$42.27^{+0.05}_{-0.04}$	$42.20^{+0.05}_{-0.04}$	$40.66^{+0.04}_{-0.05}$	$40.98^{+0.04}_{-0.05}$	$1.28^{+2.95}_{-0.94}$	$39.76^{+0.52}_{-0.58}$	$39.81^{+0.52}_{-0.58}$
J0805+2818a	$42.24^{+0.09}_{-0.07}$	$41.92^{+0.12}_{-0.09}$	$42.01^{+0.15}_{-0.11}$	$41.97^{+0.15}_{-0.11}$	$42.27^{+0.03}_{-0.03}$	$42.53^{+0.03}_{-0.03}$	$11.68^{+15.90}_{-6.95}$	$40.72^{+0.37}_{-0.39}$	$40.77^{+0.37}_{-0.39}$
J0805+2818b	< 41.87	< 41.81	< 41.71	< 41.68	$41.25^{+0.11}_{-0.15}$	$41.25^{+0.11}_{-0.15}$	$2.24^{+3.31}_{-1.38}$	$40.00^{+0.39}_{-0.41}$	$40.05^{+0.39}_{-0.41}$
J1330−0036a	< 40.90	< 40.71	< 41.05	< 41.01	$40.29^{+0.02}_{-0.02}$	$40.45^{+0.02}_{-0.02}$	$0.35^{+0.49}_{-0.21}$	$39.20^{+0.38}_{-0.39}$	$39.24^{+0.38}_{-0.39}$
J1330−0036b	$41.16^{+0.13}_{-0.10}$	$40.84^{+0.18}_{-0.13}$	$40.96^{+0.21}_{-0.14}$	$40.92^{+0.21}_{-0.14}$	$40.92^{+0.09}_{-0.11}$	$41.21^{+0.09}_{-0.11}$	$3.98^{+6.69}_{-2.57}$	$40.25^{+0.43}_{-0.45}$	$40.30^{+0.43}_{-0.45}$
J1058+3144a	< 41.32	< 41.20	< 41.30	< 41.26	$40.50^{+0.05}_{-0.06}$	$40.51^{+0.05}_{-0.06}$	$1.95^{+2.73}_{-1.19}$	$39.94^{+0.38}_{-0.41}$	$39.99^{+0.38}_{-0.41}$
J1058+3144b*	$42.61^{+0.05}_{-0.05}$	$42.12^{+0.31}_{-0.18}$	$42.61^{+0.05}_{-0.05}$	$42.47^{+0.05}_{-0.05}$	$41.02^{+0.08}_{-0.09}$	$41.24^{+0.08}_{-0.09}$	$2.44^{+5.33}_{-1.75}$	$40.04^{+0.50}_{-0.55}$	$40.09^{+0.50}_{-0.55}$
J1544+0446a	$40.49^{+0.24}_{-0.15}$	$40.35^{+0.26}_{-0.16}$	< 40.81	< 40.77	$39.82^{+0.14}_{-0.20}$	$40.16^{+0.14}_{-0.20}$	$0.37^{+1.09}_{-0.34}$	$39.22^{+0.59}_{-1.07}$	$39.27^{+0.59}_{-1.07}$
J1544+0446b*	$41.87^{+0.06}_{-0.05}$	$41.43^{+0.21}_{-0.14}$	$41.75^{+0.07}_{-0.06}$	$41.63^{+0.07}_{-0.06}$	$40.08^{+0.11}_{-0.15}$	$40.42^{+0.11}_{-0.15}$	$0.91^{+2.27}_{-0.72}$	$39.61^{+0.54}_{-0.68}$	$39.66^{+0.54}_{-0.68}$

NOTE—(2)-(4) Unabsorbed luminosity in 0.5-8 (F), 0.5-2 (S) and 2-10 keV bands. The luminosity of targets with * are derived from the fitted spectrum, while the others are converted by assuming an absorbed power-law with a photon index of 1.7 and an absorption column density $N_{\rm H} = 10^{22}$ cm^{-2}; (5) Observed luminosity in 2-10 keV bands; (6)-(7) Observed and extinction-corrected [O III] luminosity; (8) Fiber star formation rate in units of $M_\odot$ yr^{-1} given by the MPA-JHU DR7 catalog inferred from $D_n(4000)$; (9)-(10) 0.5-2 (S) and 2-10 keV bands X-ray luminosities due to star formation.

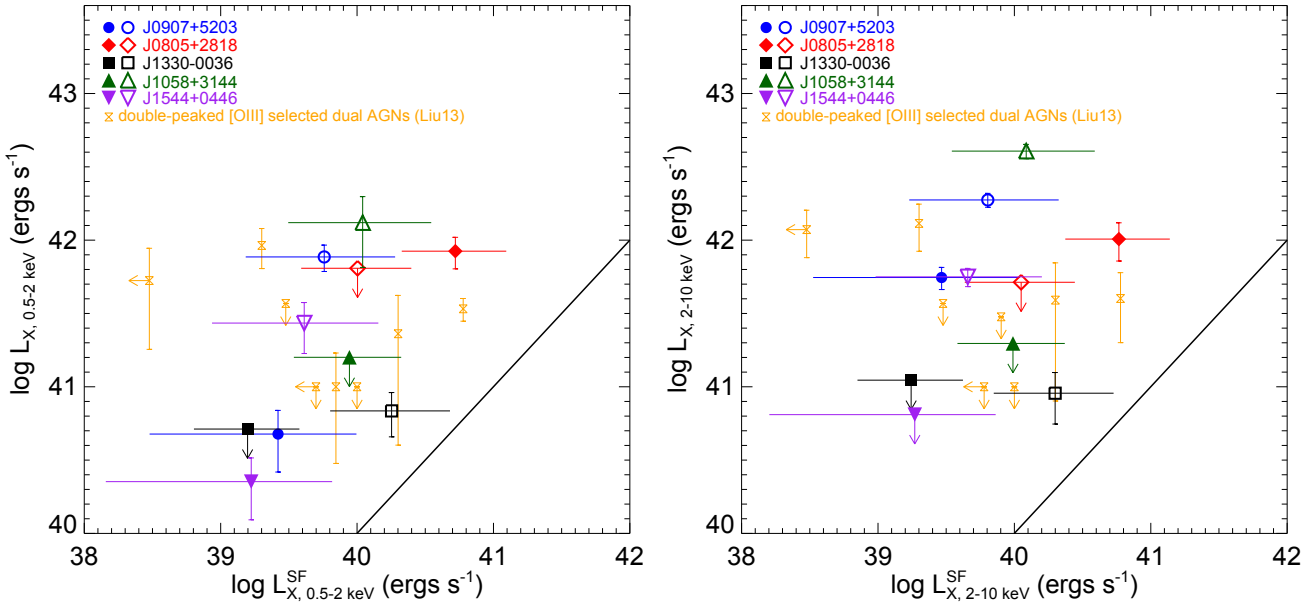
J0907+5203
J0805+2818
J1330-0036
J1058+3144
J1544+0446
double-peaked [OIII] selected dual AGNs (Liu13)
log L_X, 0.5-2 keV (ergs s^-1)
log L^SF_X, 0.5-2 keV (ergs s^-1)
log L_X, 2-10 keV (ergs s^-1)
log L^SF_X, 2-10 keV (ergs s^-1)
38
39
40
41
42
43

https://pypi.org/project/ppxf/
https://github.com/legolason/PyQSOFit

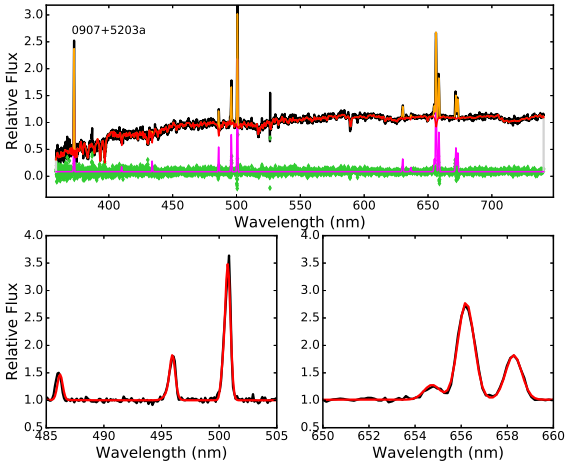
0907+5203a
Relative Flux
Wavelength (nm)

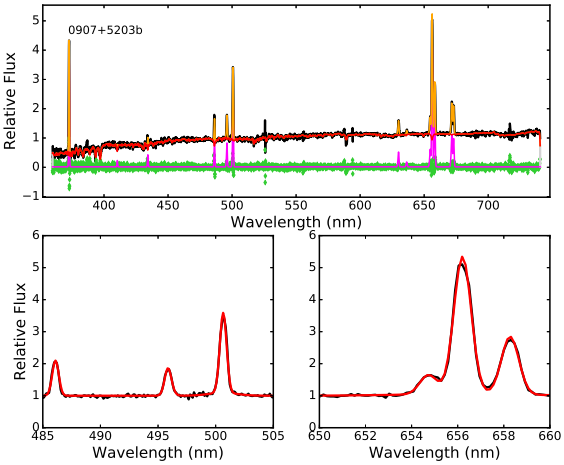
0907+5203b
Relative Flux
Wavelength (nm)

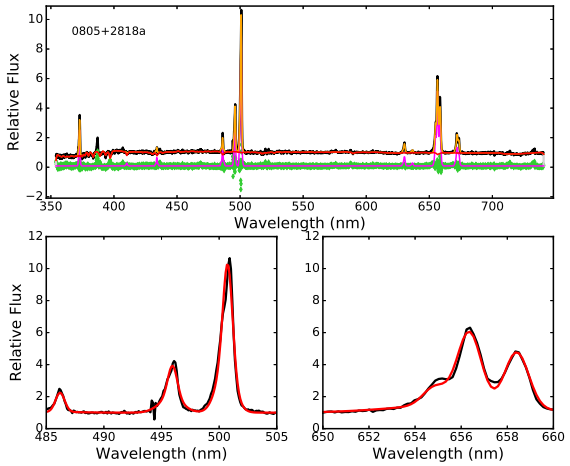
0805+2818a
Relative Flux
Wavelength (nm)

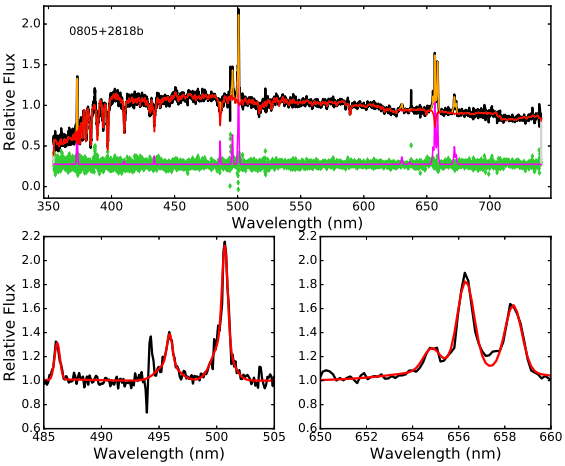
0805+2818b
Relative Flux
Wavelength (nm)

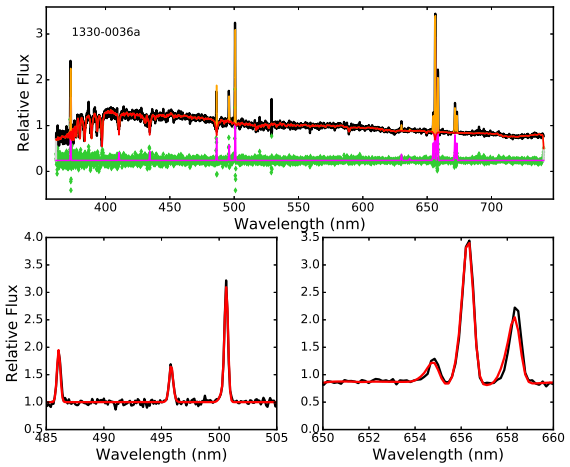
1330-0036a
Relative Flux
Wavelength (nm)

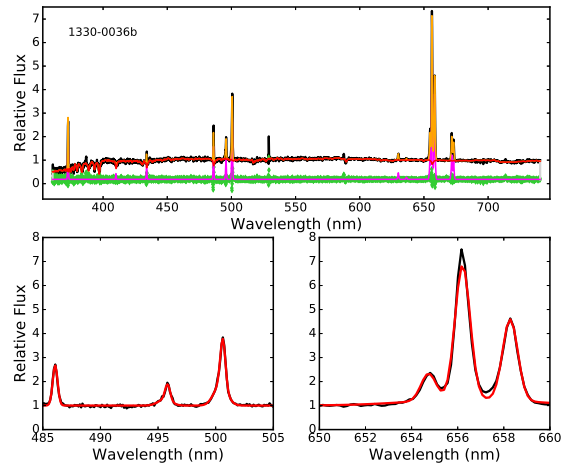
1330-0036b
Relative Flux
Wavelength (nm)

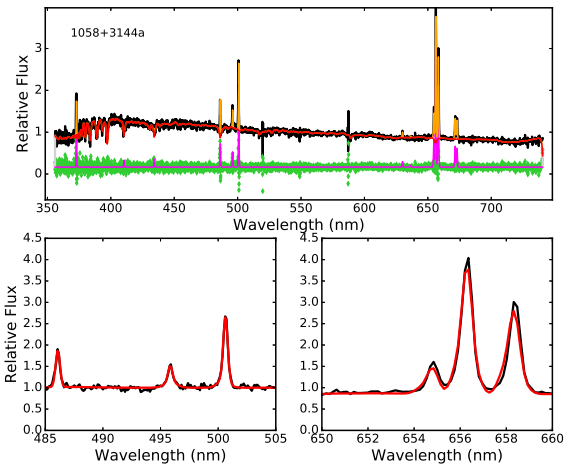
1058+3144a
Relative Flux
Wavelength (nm)
Relative Flux
Wavelength (nm)
Wavelength (nm)

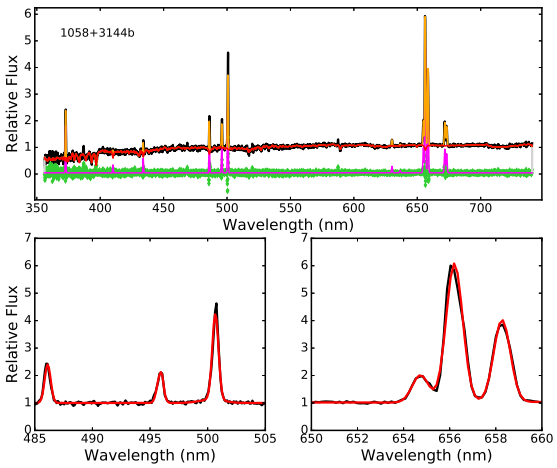
1058+3144b
Relative Flux
Wavelength (nm)
Relative Flux
Wavelength (nm)
Wavelength (nm)

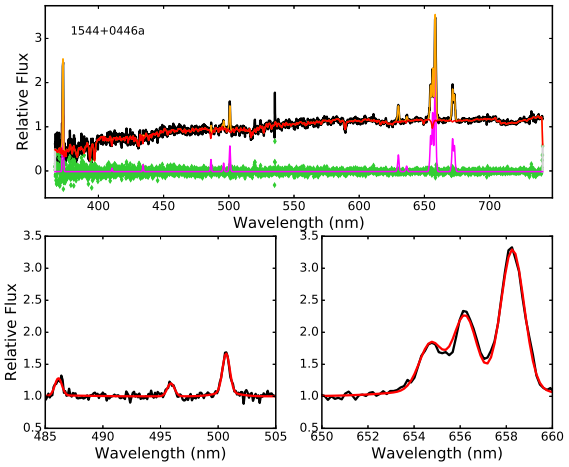
1544+0446a
Relative Flux
Wavelength (nm)
Relative Flux
Wavelength (nm)
Wavelength (nm)

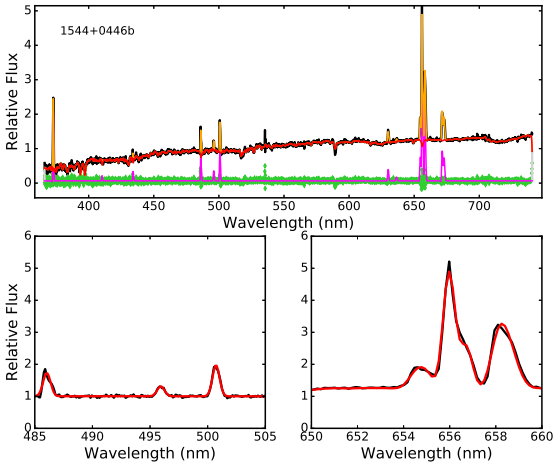
1544+0446b
Relative Flux
Wavelength (nm)
Relative Flux
Wavelength (nm)
Wavelength (nm)